Available online at www.sciencedirect.com
ScienceDirect
Journal of Power Sources 173 (2007) 1017–1023
JOURNAL OF POWER SOURCES
www.elsevier.com/locate/jpowsour

Synthesis of a novel polyaniline-intercalated layered manganese oxide nanocomposite as electrode material for electrochemical capacitor

Xiong Zhang [a], Liyan Ji [a], Shichao Zhang [b], Wensheng Yang [a,*]

[a] *State Key Laboratory of Chemical Resource Engineering, Beijing University of Chemical Technology, Beijing 100029, China*
[b] *College of Materials Science and Engineering, Beijing University of Aeronautics and Astronautics, Beijing 100083, China*

Received 30 March 2007; received in revised form 19 August 2007; accepted 28 August 2007
Available online 4 September 2007

Abstract

Polyaniline-intercalated layered manganese oxide (PANI-MnO_2) nanocomposite was synthesized via exchange reaction of polyaniline (PANI) with *n*-octadecyltrimethylammonium-intercalated manganese oxide in *N*-methyl-2-pyrrolidone solvent. The PANI-MnO_2 nanocomposite was characterized by X-ray diffraction (XRD), scanning electron microscopy (SEM), X-ray photoelectron spectroscopy (XPS), Fourier transform infrared (FTIR) spectroscopy, and so on. XRD analysis showed that the basal spacing was 1.47 nm, corresponding to the benzene rings of PANI were arranged in a zigzag conformation and located perpendicular to the inorganic layers. The C—N stretching vibration (ν_{C-N}) which appeared with PANI at 1293 cm^{-1} shifted to 1306 cm^{-1} for PANI-MnO_2 nanocomposite, indicating the existence of interactions between intercalated PANI and manganese oxide layers. The XPS results showed that PANI was still in the conductive form after inserting the polymer into layered manganese oxide. The electrochemical properties as electrode materials for electrochemical capacitors were examined by cyclic voltammetry and galvanostatic charge/discharge test in 0.1 M Na_2SO_4 solution. The maximum specific capacitance of 330 F g^{-1} was obtained from galvanostatic charge/discharge at a constant current density of 1 A g^{-1}. The specific capacitance of PANI-MnO_2 nanocomposite had improvement values of 76 and 59% compared to those of PANI (187 F g^{-1}) and manganese oxide (208 F g^{-1}) components, respectively, which was due to synergic effects from each pristine component.

Keywords: Polyaniline; Layered manganese oxide; Intercalation; Nanocomposite; Electrochemical capacitor

1. Introduction

Electrochemical capacitor, also called supercapacitor, is a kind of charge storage devices between traditional electrostatic capacitor and rechargeable battery, which can be used from mobile electronic devices to hybrid electric vehicles because of its high power density, excellent reversibility and long cyclic life [1]. The electrode materials of electrochemical capacitors can be divided into three main categories: carbon, noble/transition-metal oxides and conducting polymers. A hydrous form of ruthenium oxide has possessed a specific capacitance as high as 720 F g^{-1} and excellent cycle-life stability in aqueous H_2SO_4 [2]. However, the high cost and toxic nature of ruthenium oxide limits it from broad applications. Therefore, much research interests have been prompted to focus on other transition-metal oxides and conducting polymers. In this respect manganese oxide is one of the most attractive candidates for electrochemical capacitor electrode materials because of its environmental friendliness and low cost [3,4]. Conducting polymers such as polyaniline have also been considered as one of the most promising electrode materials for electrochemical capacitor due to their low cost, ease of synthesis, and relatively high conductivity [5]. However, comparing with ruthenium oxide, both manganese oxide and polyaniline exhibit much lower electrochemical capacitance performance.

Recently, conducting polymers-intercalated layered inorganic materials have been intensively investigated due to their potential use as electrode materials in lithium ion batteries [6–11]. The combination of two extremely different components, at the molecular level, provides a method to design new nanocomposite materials as well as the ability to improve the properties of both components. However, it is less reported to

* Corresponding author. Tel.: +86 10 64435271; fax: +86 10 64425385.
E-mail address: yangws@mail.buct.edu.cn (W. Yang).

0378-7753/$ – see front matter © 2007 Elsevier B.V. All rights reserved.
doi:10.1016/j.jpowsour.2007.08.083

use such organic–inorganic nanocomposite as electrode material for electrochemical capacitor [12,13].

The birnessite-type manganese oxide is a two-dimensional layered structure, composed of edge-shared MnO_6 octahedra, with water molecules and/or metal cations occupying the interlayer region [14]. The incorporation of polyaniline into layered manganese oxide is of interest, because the resulting nanocomposite could possess synergic properties from both components, such as enhancement in electrochemical cycling stability or electronic conductivity. In particular, both these components are expected to be electrochemical active, which may improve the electrochemical storage ability. However, birnessite-type layered manganese oxides have a high charge density in the interlayer, which makes the synthesis of layered manganese oxide nanocomposite by the conventional intercalation reaction very difficult [15]. Liu et al. prepared a layered nanocomposite with poly(diallydimethylammonium) (PDDA) cations intercalated between manganese oxide layers by a delamination/reassembling process [16]. In addition, Wang et al. applied the layer-by-layer (LBL) self-assembly technique to fabricate the ordered multilayered ultrathin films composed of manganese oxide nanosheets and PDDA ions [17]. Recently, Nakayama et al. applied a direct electrodeposition to prepare layered manganese oxide nanocomposite intercalated with PDDA polyelectrolyte [15]. However, these polyelectrolyte-intercalated layered manganese oxide nanocomposite showed poor electrochemical activity [18].

We present here another strategy for constructing birnessite-type layered manganese oxide material intercalated with conducting polymer. The process consists of incorporation polyaniline into layered manganese oxide nanocomposite via exchange reaction of polyaniline with *n*-octadecyltrimethylammoniumintercalated layered manganese oxide in *N*-methyl-2-pyrrolidone (NMP) solvent. To our knowledge, it is the first time to prepare polyaniline-intercalated layered manganese oxide nanocomposite. We also describe charge storage properties of the resulting nanocomposite in a neutral aqueous electrolyte. The high specific capacitance of $330\,F\,g^{-1}$ is obtained from galvanostatic charge/discharge at a constant current density of $1\,A\,g^{-1}$, which is much larger than that of each pristine component.

2. Experimental

2.1. Materials

Aniline of analytical grade was purchased form Beijing Chemical Reagent Corp., and distilled under vacuum prior to use. All other reagents were received as analytical grade and were used without further purification.

2.2. Synthesis of the colloidal solution of manganese oxide nanosheets

The colloidal solution of manganese oxide nanosheets was synthesized according to the method reported by Liu et al. [19]. A mixed solution of 0.6 M NaOH and 2 M H_2O_2 was quickly poured into a 0.3 M $Mn(NO_3)_2$ solution and stirred for 30 min. The precipitates were subjected to hydrothermal treatment at 150 °C for 16 h in a 2 M NaOH solution. The sodium birnessite obtained was acid treated with a 1 M HNO_3 solution for 3 days at room temperature, and then washed with water, and dried at 70 °C, which was designated as H-Birnessite. H-Birnessite (2 g) was treated in a 0.16 M aqueous solution of tetramethylammonium hydroxide (200 ml) for 7 days at 25 °C. After soaking, the suspension was centrifuged at a speed of 10,000 rpm for 10 min and washed with 200 ml distilled water four times to obtain the delaminated manganese oxide colloidal solution.

2.3. Synthesis of n-octadecyltrimethylammonium-intercalated layered manganese oxide

A certain amount of *n*-octadecyltrimethylammonium chloride aqueous solution was added into 100 ml of the colloidal solution of manganese oxide. The ratio of *n*-octadecyltrimethylammonium chloride (mol) to manganese oxide (mol) was adjusted to 0.5. After stirring 24 h at 40 °C, the reaction mixture was filtered and washed with excess of water and acetone, and then dried at 50 °C for 12 h. The product was designated as OCTA-MnO_2.

2.4. Synthesis of PANI

Aniline was dissolved in 1 M HCl and cooled to 0 °C. Ammonium peroxydisulfate (1.15 equiv.) was then added to the monomer solution. The reaction mixture was allowed to stir at ice temperature for 4 h, then filtered and washed with 1 M HCl. The dark blue product obtained was allowed to dry at 50 °C for 12 h.

2.5. Intercalation of polyaniline into layered manganese oxide

An amount of 0.25 g OCTA-MnO_2 was put into 40 ml of *N*-methyl-2-pyrrolidone (NMP) and sonicated for 60 min, while an amount of 0.05 g PANI was added to 20 ml NMP and sonicated for 60 min. The PANI-NMP colloid was added to the OCTA-MnO_2 suspension, and the reaction mixture was sonicated for 30 min. It was then allowed to stir for 24 h at 40 °C. The reaction mixture was filtered, and washed with acetone and NMP, and then the product was dried at 50 °C for 12 h. The product was designated as PANI-MnO_2.

2.6. Characterization techniques

X-ray diffraction (XRD) data were collected from a Shimadzu XRD-6000 powder diffractometer, using Cu Kα radiation (40 kV and 30 mA) between 3° and 40° with a scanning rate of $2^\circ\,min^{-1}$. The scanning electron microscope (SEM) images were taken from a Hitachi S4700 SEM. X-ray photoelectron spectroscopy (XPS) measurements were performed using a Thermo VG ESCALAB 250 instrument equipped with a monochromatic Al Kα X-ray source (1486.6 eV). To separate the different N components in the N 1s peaks, the spectrum

was fitted with three mixed Gaussian/Lorentzian peaks. The peak position and width, as well as the ratio of the Gaussian and Lorentzian components (G/L), were all allowed to vary freely, but the width and the G/L ratio of the peaks were set to be equal in each fit. Fourier transform infrared (FTIR) spectra were recorded on a Brucker Vector 22 spectroscopic by the KBr method. Compositional analysis was performed by inductively coupled plasma emission spectroscopy (ICP-ES) using a Shimadzu ICPS-7500 instrument. C, H and N microanalysis was recorded on an Elementar Vario El elemental analyzer. Thermogravimetry (TG) analysis was carried out on a Perkin-Elmer Diamond analyzer with N_2 gas. Samples were heated from 30 to 800 °C at a rate of 10 °C min^{-1}. Electronic conductivity was measured on compacted pellets using a four-probe conductivity method.

2.7. Electrochemical measurements

The electrode performance was measured in a beaker-type electrochemical cell equipped with the working electrode, a platinum counter electrode, and a standard calomel electrode (SCE) as reference electrode. The working electrode was prepared by mixing 70 wt.% active material, 20 wt.% acetylene black and 10 wt.% PVdF in NMP and the slurry was spread onto a nickel sheet with 1 cm^2 geometry area. The electrode was heated at 100 °C for 2 h to evaporate solvent. The mass of active material on the working electrode was in the range of 0.35–0.40 mg cm^{-2}. The electrolyte was 0.1 M Na_2SO_4 aqueous solution. Cyclic voltammetry scans were recorded from 0 to 0.85 V at a scan rate of 5 mV s^{-1}, using ZAHNER IM6e electrochemical workstation. Galvanostatic charge/discharge cycling in the potential range of 0–0.85 V (vs. SCE) was performed at a constant current density of 1 A g^{-1}.

3. Results and discussion

3.1. XRD

Fig. 1 shows the XRD patterns of H-Birnessite, OCTA-MnO_2 and PANI-MnO_2 nanocomposite. H-Birnessite has a layered structure with a basal spacing of 0.73 nm (Fig. 1a). H-Birnessite product was treated in tetramethylammonium hydroxide solutions for 7 days and centrifuged, washed with distilled water four times to obtain the delaminated manganese oxide colloidal solution. The XRD pattern of the delaminated manganese oxide colloidal solution gives no diffraction features but only an amorphous halo, which is similar to the case of Liu's report in the previous paper [19]. When the *n*-octadecyltrimethylammonium chloride aqueous solution was added into the delaminated manganese oxide colloidal solution, it shows a new phase with a basal spacing of 3.24 nm for the OCTA-MnO_2 product. The XRD pattern consisted of a well-resolved 0 0 *l* basal series in the low 2θ range suggests that the manganese oxide layers are restacked in an ordered manner. Since the distance between two adjacent carbon atoms can be expressed by 0.13 nm/CH_2 in the all-*trans* extended alkyl chains [20], the length of *n*-octadecyltrimethylammonium is estimated to be 2.79 nm. The

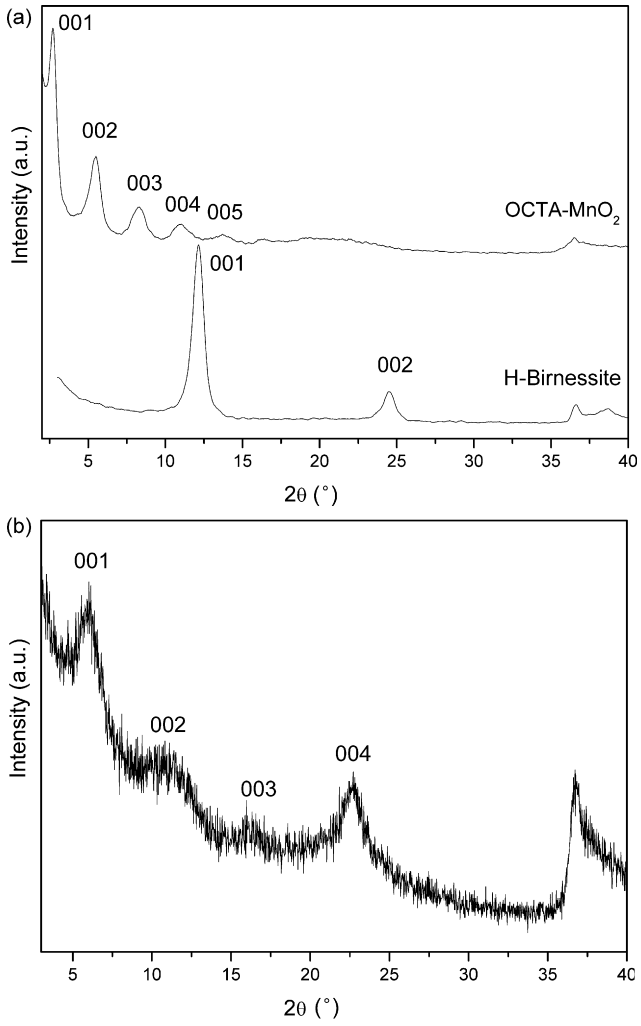

Fig. 1. (a) X-ray diffraction patterns of H-Birnessite and OCTA-MnO_2 and (b) X-ray diffraction pattern of PANI-MnO_2 nanocomposite.

value of the expansion of the interlayer is about 2.79 nm (the basal spacing minus the thickness of the manganese oxide layer, 0.45 nm [19]), which is much compatible with a layer of *n*-octadecyltrimethylammonium ions in which the head groups are organised head-to-tail, leading to an interdigitated arrangement of the hydrocarbon tails [21]. Elemental analysis gives C 35.0%, H 7.3%, N 2.1%, Mn 32.5%, O balance, which suggests the formula $(C_{21}H_{40}N)_{0.18}MnO_2{\cdot}0.67H_2O$. The water content is calculated from the weight loss by the TG curve. The C/N molar ratio is 19.4, which is close to the C/N molar ratio (C/N = 21) of the *n*-octadecyltrimethylammonium ion. This indicates that the organic component in the interlayer consists mainly of the *n*-octadecyltrimethylammonium ions.

After the reaction between PANI and OCTA-MnO_2 in NMP, the diffraction peaks of the OCTA-MnO_2 product are completely disappeared and a new basal spacing of 1.47 nm is observed. After subtracting the thickness of the manganese oxide layer, the net interlayer expansion is about 1.02 nm. This expansion is reasonable for intercalation of a monolayer of PANI molecules, which suggested that the benzene rings of PANI are arranged in a zigzag conformation and located perpendicular to the inorganic

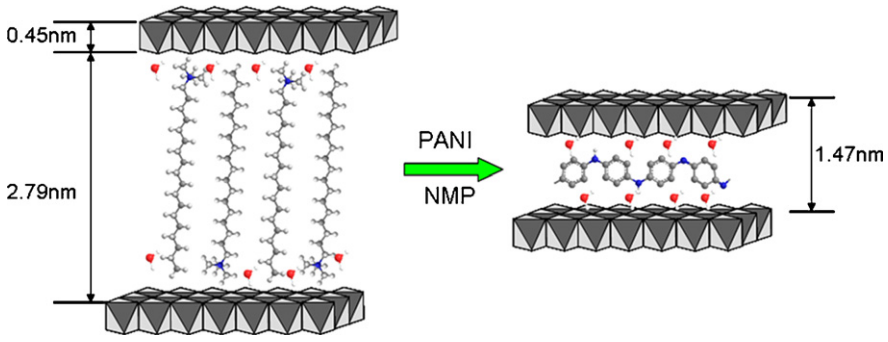

Fig. 2. Schematic illustration for the formation of PANI-intercalated manganese oxide.

layers. A similar arrangement was observed for PANI intercalated in α-$RuCl_3$ [22] and FeOCl [23]. Elemental analysis gives C 25.1%, H 4.5%, N 5.3%, Mn 37.4%, O balance, and the C/N molar ratio is 5.5. A schematic illustration for the formation of PANI-intercalated manganese oxide nanocomposite is shown in Fig. 2.

3.2. SEM

SEM images of OCTA-MnO_2, and PANI-MnO_2 nanocomposite are presented in Fig. 3a and b, respectively. It is apparent that OCTA-MnO_2 product comprises of plate-like particles, which are about 50 nm in thickness and 200–500 nm in lateral dimensions. After polyaniline being intercalated between manganese oxide layers, the mophology of product are maintained. This composite material in nano-size should give the opportunity of obtaining enhanced capacitance due to surface effects.

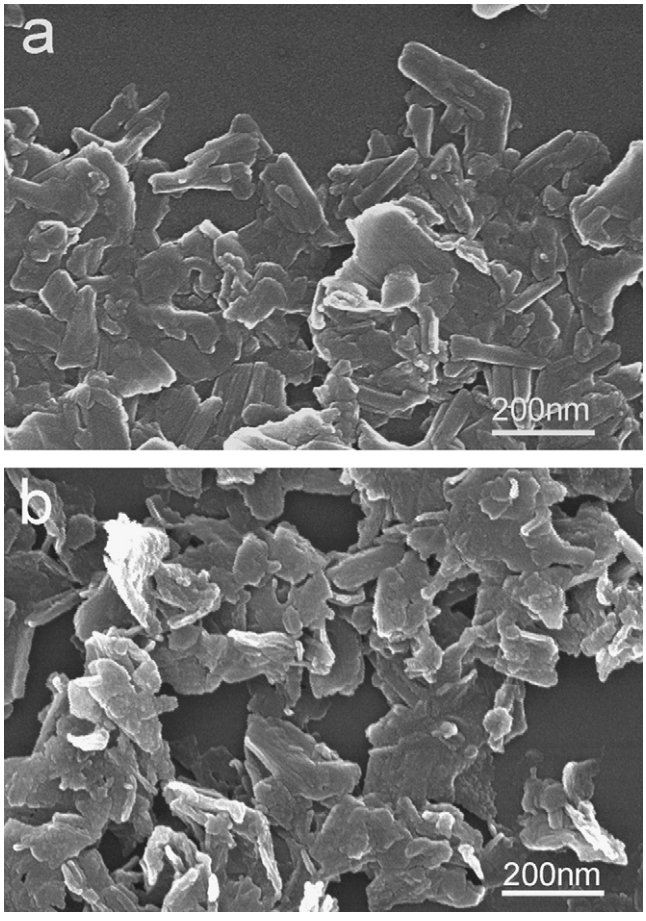

Fig. 3. SEM micrographs of (a) OCTA-MnO_2 and (b) PANI-MnO_2.

3.3. FTIR

The FTIR spectra of OCTA-MnO_2, PANI and PANI-MnO_2 nanocomposite are given in Fig. 4, respectively. Bands around 3400 and 1630 cm^{-1} are observed for OCTA-MnO_2 and PANI-MnO_2 product, due to the presence of interlayer or surface water [16]. The bands around 505 and 440 cm^{-1} are corresponding to Mn–O stretching vibrations [24]. OCTA-MnO_2 shows the characteristic absorption bands due to the C–H asymmetric and C–H symmetric stretching frequencies (2915 and 2847 cm^{-1}, respectively), CH_2 bending vibrations (1471, 1400, 960, and 910 cm^{-1}), and C–N symmetric stretching vibration (1046 cm^{-1}). The characteristic absorption bands of PANI appear at 1293 and 1569 cm^{-1}, corresponding to the stretching mode of C–N and C=N bands, reveal the presence of leucoemeraldine and permigraniline components [25]. FTIR spectrum of the PANI-MnO_2 nanocomposite exhibits characteristic bands of PANI as well as of manganese oxide, which confirms the presence of both components in the nanocompos-

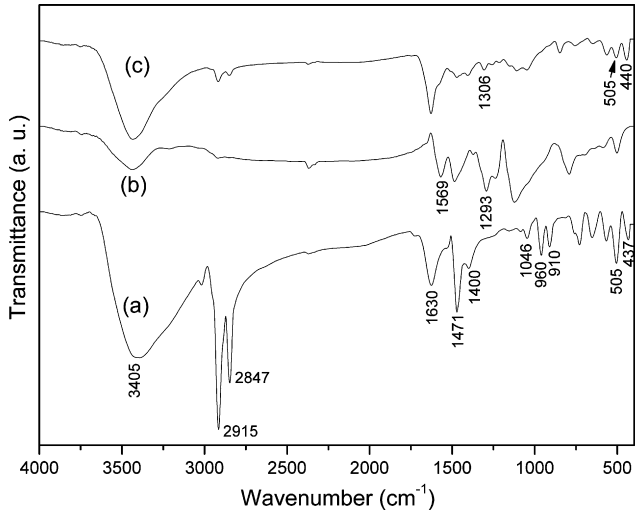

Fig. 4. FTIR spectra of (a) OCTA-MnO_2, (b) PANI and (c) PANI-MnO_2.

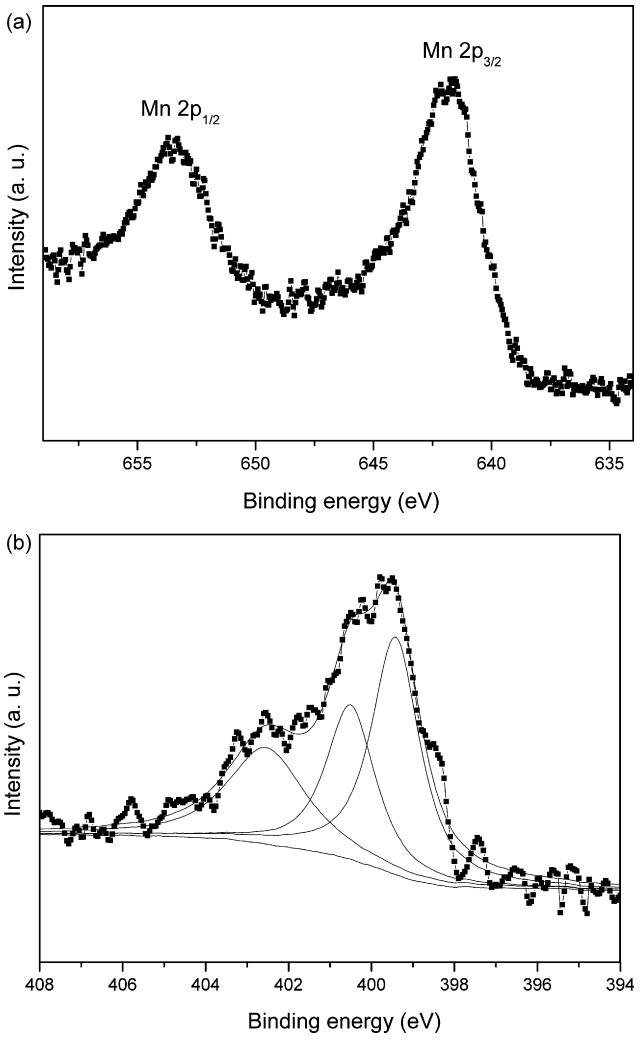

Fig. 5. Mn 2p XPS spectrum (a) and N 1s XPS spectrum (b) for PANI-MnO_2 nanocomposite.

ite. The stretching mode of C–N band is shift to 1306 cm^{-1} due to the physicochemical interaction between the intercalated PANI and manganese oxide layers [26].

3.4. XPS and electronic conductivity

The PANI-MnO_2 nanocomposite is subjected to XPS analysis and the results from Mn 2p and N 1s core levels of the above samples are shown in Fig. 5. The Mn 2p region consists of a spin-orbit doublet with Mn $2p_{1/2}$ having a binding energy of 653.3 eV and Mn $2p_{3/2}$ with a binding energy of 641.7 eV (Fig. 5a), which are characteristic of a mixed-valence manganese system (Mn^{4+} and Mn^{3+}) [27]. The N 1s spectral envelope clearly results from more than a single type of nitrogen (Fig. 5b). A minimum of three peaks are required to adequately decompose the spectral envelope using a mixed Gaussian and Lorentzian function. The peak at around 399.4 eV is attributed to the amine nitrogen of the polymer while the other two peaks at 400.5 and 402.5 eV correspond to positively charged nitrogen. These two different environments at >400 eV can be interpreted as polaron and bipolaron states, respectively. Doping level is often determined as the area ratios of the peaks >400 eV with respect to total nitrogen [28,29]. In this work, calculation of the [N+]/[N] ratio from the spectral decomposition indicates a doping level of 0.6 for the PANI intercalated into layered manganese oxide, suggesting a high level of doping in PANI. Therefore, PANI is still in the conductive form after inserting the polymer into layered manganese oxide. The room temperature conductivities of PANI, H-Birnessite and PANI-MnO_2 samples are 4.22×10^{-1}, 4.83×10^{-2} and 1.08×10^{-1} S cm^{-1}, respectively. The electronic conductivity of PANI-MnO_2 nanocomposite is two times higher than that of pristine manganese oxide, which indicates that intercalation of PANI into layered manganese oxide can improve the conductivity of manganese oxide.

3.5. TG analysis

Fig. 6 shows the TG curves of OCTA-MnO_2, PANI-MnO_2 and PANI, respectively. According to the TG curve of OCTA-MnO_2 (Fig. 6a), a weight loss of 7% up to 170 °C is due to the removal of physically adsorbed and interlayer water. A sharp weight loss (32%) from 170 to 268 °C is attributed to the decomposition of *n*-octadecyltrimethylammonium ions in the interlayer. The further decomposition of organic ions (18%) is occurred at 268–500 °C. A small weight loss (3%) between 500 and 800 °C is due to the reduction of manganese from tetravalent to trivalent form accompanied by the evolution of oxygen [16]. In the TG curve of PANI-MnO_2 (Fig. 6b), a weight loss of 4.8% up to 130 °C is due to the dissipation of the interlayer water. A further weight loss (33.1%) observed from 130 to 600 °C is attributed to the decomposition of PANI in the interlayer. The weight loss is close to the PANI contents of PANI-MnO_2 nanocomposite (34%) calculated by using the elemental analysis. On the other hand, the thermal stability of PANI in PANI-MnO_2 nanocomposite has decreased compared to pure PANI (Fig. 6c), suggesting the activation of PANI decomposition by manganese oxide inorganic lattice.

3.6. Electrochemical characterization

Cyclic voltammetry (CV) and galvanostatic charge/discharge test were employed to characterize the electrochemical capacitance performance of PANI-MnO_2 nanocomposite. Fig. 7 shows the cyclic voltammograms of H-Birnessite, pure PANI and PANI-MnO_2 nanocomposite electrodes with sweep rate of 5 mV s^{-1} in a potential range between 0 and 0.85 V (vs. SCE). The CV curves of H-Birnessite and PANI-MnO_2 nanocomposite show roughly rectangular mirror images with respect to the zero-current line, indicating the capacitive behaviors. It can be seen clearly that there are no redox peaks in the working potential. However, the pure PANI has poor capacitive behavior in the potential range between 0 and 0.85 V.

Fig. 8 shows the charge/discharge curves of pure PANI, H-Birnessite and PANI-MnO_2 nanocomposite electrodes. H-Birnessite and PANI-MnO_2 nanocomposite indicate good capacitive behavior at a current density of 1 A g^{-1}. For pure PANI, the *iR* drop (*iR* drop is defined as the electrical potential

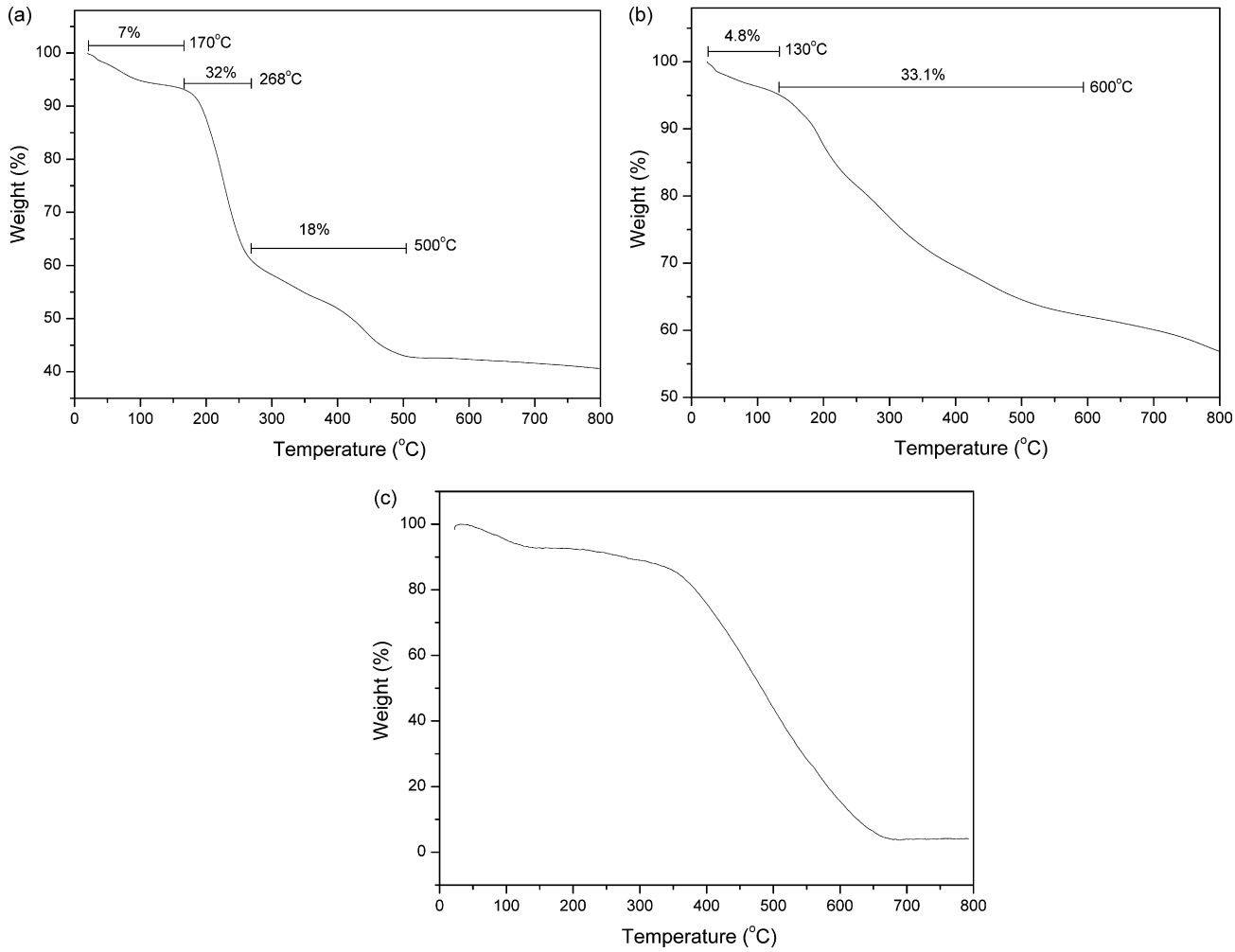

Fig. 6. TG curves of (a) OCTA-MnO_2, (b) PANI-MnO_2 and (c) PANI.

difference between the two ends of a conducting phase during a current flow and is the product of the current (i) and the resistance (R) of the conductor [30]) during the charge/discharge test is more obvious. However, the charge/discharge curve of PANI-MnO_2 nanocomposite shows less iR drop. The obtained charge/discharge curves are used for the calculation of specific capacitance from the equation:

$$C = \frac{I}{(\mathrm{d}V/\mathrm{d}t)m} \quad (1)$$

where $\mathrm{d}V/\mathrm{d}t$ is the slope of the linear discharge curve, I the current, and m is the mass of active material within the electrode.

The specific capacitance values calculated from the charge/discharge curves are 187, 208, 330 F g^{-1} for pure PANI, H-Birnessite and PANI-MnO_2 nanocomposite, respectively. The specific capacitance of PANI-MnO_2 nanocomposite is much larger than that of each pristine component. The enhanced specific capacitance may be attributed to the higher electronic conductivity and the enhanced bidimensionality [10].

The electrochemical stabilities of PANI, H-Birnessite and PANI-MnO_2 nanocomposite were examined by means of cycle-life test at a current density of 1 A g^{-1}. The cyclic performances of PANI, H-Birnessite and PANI-MnO_2 nanocomposite electrodes are shown in Fig. 9. After 1000 cycles of operation, the electrodes can maintain ~75, ~90, and ~94% of their initial capacitances for PANI, H-Birnessite and PANI-MnO_2 nanocomposite, respectively. This result indicates that such PANI-MnO_2

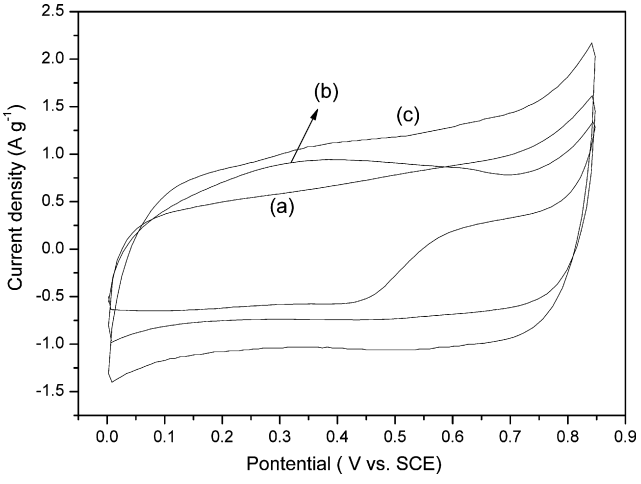

Fig. 7. Cyclic voltammograms of H-Birnessite (a), pure PANI (b) and PANI-MnO_2 nanocomposite (c) electrodes. Electrodes are scanned in a potential range of 0–0.85 V (vs. SCE). The scan rate is 5 mV s^{-1}.

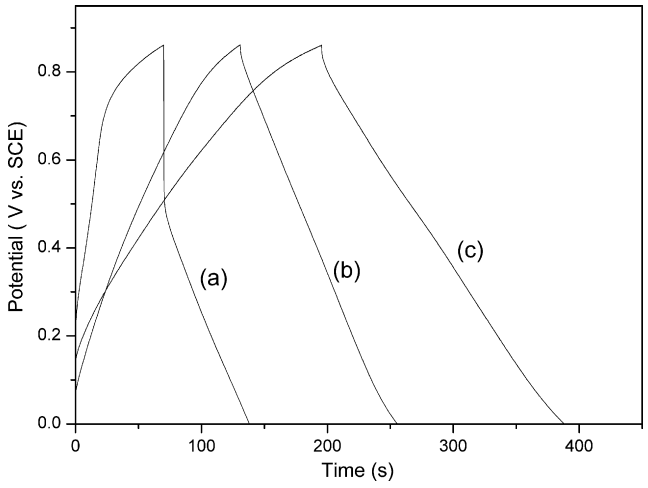

Fig. 8. Charge/discharge curves of pure PANI (a), H-Birnessite (b) and PANI-MnO_2 nanocomposite (c) electrodes in the potential range of 0–0.85 V (vs. SCE). The current density is 1 A g^{-1}.

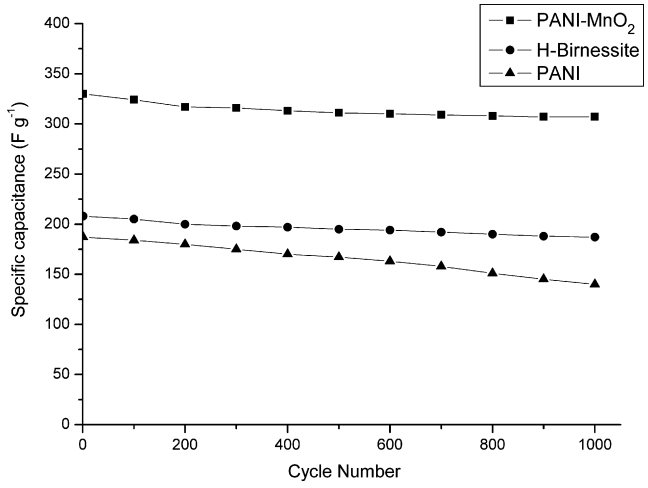

Fig. 9. Cyclic performances of PANI, H-Birnessite and PANI-MnO_2 nanocomposite electrodes in the voltage range of 0–0.85 V (vs. SCE).

nanocomposite has a good long-term electrochemical stability at a relatively high current density.

4. Conclusion

A novel polyaniline-intercalated layered manganese oxide nanocomposite is synthesized through ion-exchange reaction between *n*-octadecyltrimethylammonium-intercalated precursors and polyaniline in an organic solution. The value of the basal spacing suggests that the benzene rings of PANI are arranged in a zigzag conformation and located perpendicular to manganese oxide layers. The specific capacitance for PANI-MnO_2 electrode is about 330 F g^{-1} at a charge/discharge current density of 1 A g^{-1} in 0.1 M Na_2SO_4 solution. The specific capacitance of PANI-MnO_2 nanocomposite can maintain 94% of initial specific capacitance after 1000 cycles. The polyaniline-intercalated layered manganese oxide nanocomposite shows not only the enhancement of specific capacitance, but also the improvement of electrochemical cyclic stability compared with those of pristine polyaniline and manganese oxide. The synthetic strategy for constructing nanocomposite electrode material can be extended to other conductive polymers such as polypyrrole and polythiophene.

Acknowledgements

This research was supported by the National Natural Science Foundation of China (Grant No. 20301002), the Ministry of Science and Technology High Technology Development 863 Plan (Grant No. 2006AA03Z343), and the 111 Project (Grant No. B07004).

References

[1] R. Kötz, M. Carlen, Electrochim. Acta 45 (2000) 2483.
[2] J.P. Zheng, T.R. Jow, J. Electrochem. Soc. 142 (1995) L6.
[3] C.-C. Hu, T.-W. Tsou, Electrochem. Commun. 4 (2002) 105.
[4] Y. Dai, K. Wang, J. Zhao, J. Xie, J. Power Sources 161 (2006) 737.
[5] Y.-G. Wang, H.-Q. Li, Y.Y. Xia, Adv. Mater. 18 (2006) 2619.
[6] P. Gomez-Romero, Adv. Mater. 13 (2001) 163.
[7] G.R. Goward, F. Leroux, L.F. Nazar, Electrochim. Acta 43 (1998) 1307.
[8] S.-G. Kang, K.M. Kim, N.-G. Park, K.S. Ryu, S.-H. Chang, J. Power Sources 133 (2004) 263.
[9] A.V. Murugan, C.W. Kwon, G. Campet, B.B. Kale, A.B. Mandale, S.R. Sainker, C.S. Gopinath, K. Vijayamohanan, J. Phys. Chem. B 108 (2004) 10736.
[10] A.V. Murugan, M. Quintin, M.-H. Delville, G. Campet, K. Vijayamohanan, J. Mater. Chem. 15 (2005) 902.
[11] G. Wang, Z. Yang, X. Li, C. Li, Carbon 43 (2005) 2564.
[12] A.V. Murugan, A.K. Viswanath, G. Campet, C.S. Gopinath, K. Vijayamohanan, Appl. Phys. Lett. 87 (2005) 243511.
[13] A.V. Murugan, A.K. Viswanath, C.S. Gopinath, K. Vijayamohanan, J. Appl. Phys. 100 (2006) 074319.
[14] Q. Feng, H. Kanoh, K. Ooi, J. Mater. Chem. 9 (1999) 319.
[15] M. Nakayama, H. Tagashira, S. Konishi, K. Ogura, Inorg. Chem. 43 (2004) 8215.
[16] Z. Liu, X. Yang, Y. Makita, K. Ooi, Chem. Mater. 14 (2002) 4800.
[17] L. Wang, Y. Omomo, N. Sakai, K. Fukuda, I. Nakai, Y. Ebina, K. Takada, M. Watanabe, T. Sasaki, Chem. Mater. 15 (2003) 2873.
[18] M. Nakayama, H. Tagashira, Langmuir 122 (2006) 3864.
[19] Z. Liu, K. Ooi, H. Kanoh, W. Tang, T. Tomida, Langmuir 16 (2000) 4154.
[20] Y. Kamiya, N. Yamamoto, H. Imai, S. Komai, T. Okuhara, Micropor. Mesopor. Mater. 81 (2005) 49.
[21] E. Wortham, B. Bonnet, D.J. Jones, J. Rozière, G.R. Burns, J. Mater. Chem. 14 (2004) 121.
[22] L. Wang, M. Rocci-Lane, P. Brazis, C.R. Kannewurf, Y. Kim, W. Lee, J.-H. Choy, M.G. Kanatzidis, J. Am. Chem. Soc. 122 (2000) 6629.
[23] C.-G. Wu, D.C. DeGroot, H.O. Marcy, J.L. Schindler, C.R. Kannewurf, T. Bakas, V. Papaefthyymiou, W. Hirpo, J.P. Yesinowski, Y.-J. Liu, M.G. Kanatzidis, J. Am. Chem. Soc. 117 (1995) 9229.
[24] X. Yang, Y. Makita, Z. Liu, K. Sakane, K. Ooi, Chem. Mater. 16 (2004) 5581.
[25] Z. Niu, Z. Yang, Z. Hu, Y. Lu, C.C. Han, Adv. Funct. Mater. 13 (2003) 949.
[26] H.V. Hoang, R. Holze, Chem. Mater. 18 (2006) 1976.
[27] M. Chigane, M. Ishikawa, J. Electrochem. Soc. 147 (2000) 2246.
[28] I. Karatchevtseva, Z. Zhang, J. Hanna, V. Luca, Chem. Mater. 18 (2006) 4908.
[29] M.G. Han, S.K. Cho, S.G. Oh, S.S. Im, Synth. Mater. 126 (2002) 53.
[30] V. Subramanian, H. Zhu, B. Wei, Electrochem. Commun. 8 (2006) 827.